# Soft Matter

www.softmatter.org

Volume 4 | Number 7 | 7 July 2008 | Pages 1329–1540

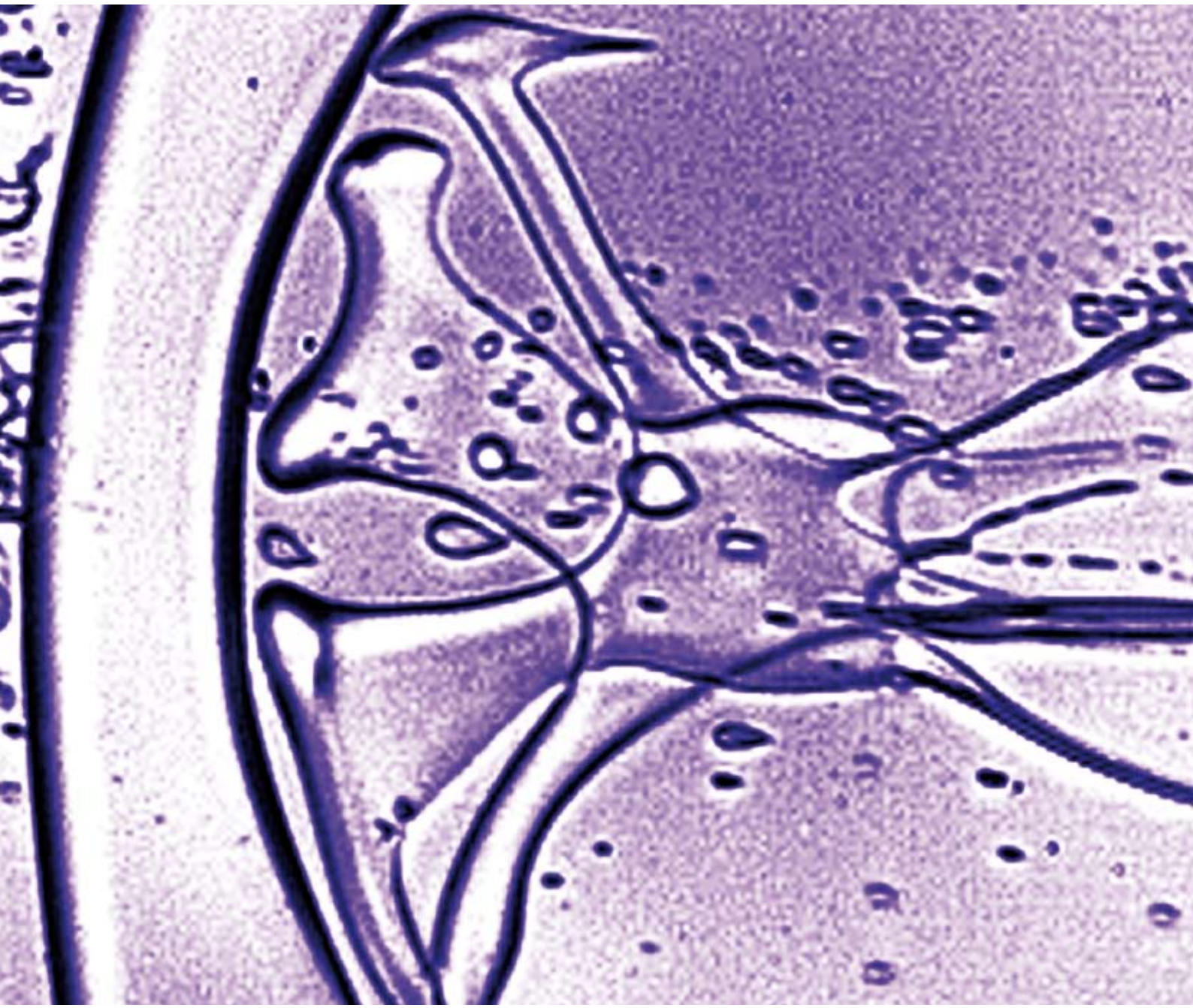

ISSN 1744-683X

RSC Publishing

**PAPER**
George M. Whitesides *et al.*
Interfacial instabilities in a microfluidic Hele-Shaw cell

**REVIEW ARTICLE**
Dirk Pijper and Ben L. Feringa
Control of dynamic helicity at the macro- and supramolecular level

1744-683X(2008)4:7;1-H

# Interfacial instabilities in a microfluidic Hele-Shaw cell†

**Michinao Hashimoto,[a] Piotr Garstecki,*[b] Howard A. Stone[c] and George M. Whitesides*[a]**

***Received 15th October 2007, Accepted 14th April 2008***
***First published as an Advance Article on the web 8th May 2008***
**DOI: 10.1039/b715867j**

This paper describes surfactant-sensitive, dynamic instabilities that occur to aqueous droplets translating in a continuous flow of hexadecane in a microfluidic Hele-Shaw cell (HSC). A very low interfacial tension (on the order of 0.01 mN $m^{-1}$) between water and hexadecane allowed for deformation of the droplets along the fields of flow and tip-streaming from moving droplets. In the system of water and hexadecane that we investigated, the use of surfactants in both fluids was necessary to achieve interfacial tension sufficiently low for the instabilities to occur. The droplets entering the HSC stretched orthogonally to the main direction of flow into elongated shapes, with aspect ratios greater than ten to one (width to length). These droplets exhibited two types of instabilities. The first included elongation of droplets, and Rayleigh–Plateau instabilities in the stretched droplets. Arrays of these stretched droplets formed three characteristic patterns that depended on the rates of flow of water and hexadecane. The second was driven by the shear stress exerted on the interface between the two fluids by the top and bottom boundaries of the HSC; this instability is named a "shear-driven instability" (SDI). Our observations supported that the SDI—an effect similar to tip-streaming—resulted from a redistribution of surfactants at the interface between the two fluids.

## Introduction

We report experimental observations of flow patterns and dynamic instabilities of droplets in a microfluidic Hele-Shaw cell.[1] The system comprises a microfluidic flow-focusing (FF) structure that generates droplets of aqueous solutions in an organic continuous phase,[2–4] and delivers the two phases into a channel that is typically fifty times wider than it is tall. We followed convention and called this channel a Hele-Shaw cell (HSC). The flow entering the HSC is characterized by a pattern of streamlines that diverges from the centerline to the sides of the cell. We studied the flow pattern of droplets of water containing Tween 20 (2% w/w) in a continuous phase of hexadecane containing Span 80 (3% w/w). With this combination of fluids and surfactants, the interfacial tension between the two fluids was extremely low (on the order of 0.01 mN $m^{-1}$), and the interface between the two fluids yielded easily to the flow field defined by the geometry of the channel; droplets elongated into sausage-like shapes with widths much larger (typically by more than a factor of ten) than their lengths as they entered the HSC. These elongated droplets experienced a capillary instability, and broke up into droplets of nearly circular cross-sections in the plane of the HSC,[5,6] with diameters comparable to the height of the HSC. The progression of the capillary instability was slowed by confinement by the boundaries of the HSC.[7,8] At low rates of flow of the two fluids, the elongated droplets flowed downstream in the form of regular 'fishbone' patterns, before breaking up into smaller drops. As we demonstrate, the shape of these patterns could be, to some extent, controlled by modifying the shape of the walls of the HSC.

Over a range of rates of flow of both phases, the droplets translating in the HSC developed 'curtains'—wide sheets of liquid—at their trailing edges, at both the floor and the ceiling of the HSC. These curtains subsequently evolved into threads, and the threads broke up into small droplets. The size of these small droplets was at least an order of magnitude smaller than the height of the HSC. On the basis of observations made in experiments with different concentrations of surfactants in both the continuous and the dispersed phase, we believe that this shear-driven instability (SDI) is critically dependent on the interfacial tension between the two phases, and on the dynamic effects of interfacial tension caused by redistribution of surfactants.

### Hele-Shaw cell

The term "Hele-Shaw cell (HSC)" refers to a space created by the gap between two parallel plates.[1] This setup has two characteristics that make it a useful tool with which to analyze multiphase flows and various interfacial phenomena. First, multiphase flows in an HSC are easily visualized through the transparent cell. Second, due to the high ratio of the lateral dimensions to the height of the cell, many flows can be well approximated by a two-dimensional description. Such two-dimensional flows in an HSC obey Darcy's law; this flow is mathematically equivalent to that in a porous medium.[9] The study of flow in an HSC thus provides insights into multiphase flows in porous media—a subject that is important in areas such as geophysics and oil recovery.[10,11] We can construct such a Hele-Shaw cell by separating two transparent plates with narrow spacers that define the aspect ratio of

[a]*Department of Chemistry and Chemical Biology, Harvard University, 12 Oxford St., Cambridge, MA, 02138, USA. E-mail: gwhitesides@gmwgroup.harvard.edu*
[b]*Institute of Physical Chemistry, Polish Academy of Sciences, Kasprzaka 44/52, 01-224 Warsaw, Poland. E-mail: garst@ichf.edu.pl*
[c]*School of Engineering and Applied Sciences, Harvard University, 29 Oxford St., Cambridge, MA, 02138, USA*

† Electronic supplementary information (ESI) available: Additional images and discussions on formation of patterns, shear-driven instability, and effects of surfactants are presented. See DOI: 10.1039/b715867j

the cell. Alternately, the use of techniques in soft lithography makes it possible to create such high aspect ratio geometries at the micron-scale.

Here we investigated flows and interfacial phenomena of aqueous droplets in an organic fluid using microfluidic versions of HSCs. Such multiphase, droplet-based systems are common in microfluidics; examples include systems used for micro-reactions,[12,13] kinetic analyses,[14] encapsulations,[15,16] syntheses of colloidal particles,[17,18] and crystallization of proteins.[19] The use of surfactants is often necessary for applications of such droplet-based systems; it is therefore important to understand the behaviors of droplets and the influence of surfactants at length-scales relevant to on-chip applications.

### Instabilities in a Hele-Shaw cell

Instability, the spontaneous transition of one type of flow to another, is ubiquitous in the studies of flows of fluids. The Saffman–Taylor instability in an HSC and a porous medium—an instability that develops when a less viscous fluid displaces a more viscous one—has received much attention after the original description by Hill and then Saffman and Taylor in the 1950's.[20,21] Krechetnikov and Homsy recently reported a novel observation, called a 'reversed' Saffman–Taylor instability; they reported that the replacement of a less viscous fluid with a more viscous fluid in an HSC also led to an instability when the walls of the HSC were pre-wetted with the surfactant-rich, less viscous fluid.[22] The presence of surfactant was a necessary condition for the onset of this instability. Importantly, while the classic Saffman–Taylor instability could be described within a two-dimensional model (Darcy's equation), the observations of Krechetnikov and Homsy also included the flow in the third dimension (that is, perpendicular to the plane on the HSC). In this report, we discuss a surfactant-sensitive instability (which we call "shear-driven instability" or SDI) that reflects the three-dimensional pattern of flows between the droplets; convective flows between the translating droplets shear surfactants along the top and bottom of an HSC.

The capillary instability, also called the Rayleigh–Plateau instability, has been studied extensively since first Plateau and then Rayleigh reported the break-up of long threads of fluid placed in a second, immiscible fluid.[5,6] The groups of Son and Pathak reported the effects of confinement on the capillary instability.[7,8] Our observations confirmed their findings; when the immiscible threads were confined between two parallel plates (the boundaries of the HSC), either the capillary instability progressed at a rate that was slower than that in an unbounded fluid, or did not occur at all. Here we demonstrated that this suppression of break-up of stretched droplets, when combined with a flow in an HSC, could generate highly regular patterns of elongated droplets and small daughter droplets.

Redistribution of surfactants on the surface of droplets under shear is another problem of interest. When a droplet is located in an external flow field, the flow field affects the shape of the droplet (as originally described by Taylor, where a droplet was located in linear extensional flows).[23] Stone and Leal and then Eggleton *et al.* studied a droplet containing surfactants placed in the same extensional flow fields as Taylor's original study.[24–27] The result of the computer simulations showed that the field created a region at the tips of droplets that was high in the concentration of surfactant; these tips developed highly pointed cusps that emitted streams of smaller daughter droplets.[27] Our current work provided experimental demonstrations of tip-streaming by shearing in the confined geometry of the HSC. We observed that the onset of the tip-streaming was sensitive to the concentrations of the surfactants in *both* the droplet phase and the continuous phase.

## Experimental design

### Design of the device

The microfluidic flow-focusing generator makes it possible to form monodisperse droplets repeatedly over time.[3] We used a planar, monolithic microfluidic flow-focusing device to form droplets *in situ*, and delivered them into an HSC; the HSC directly followed the flow-focusing generator of droplets in the fluidic stream. Fig. 1a illustrates our experimental system schematically. We used standard techniques of soft lithography to fabricate microfluidic devices.[28] Soft lithographic techniques offered three advantages. First, we had flexibility in designing the

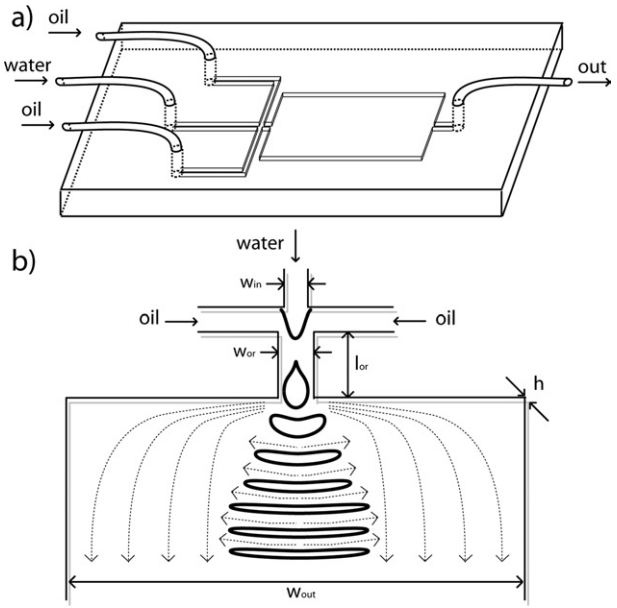


**Fig. 1** a) Schematic illustration of the experimental system used in our study. A polydimethylsiloxane (PDMS) slab having the channels embossed in its surface is sealed against a flat PDMS slab. We delivered the fluids from syringe pumps through polyethylene terephthalate tubing. b) Top view of the flow-focusing region and the entry to the outlet channel. Bold solid lines represent droplets, and the dashed lines represent the streamlines of the continuous fluid. The flow of the continuous fluid to the sides of the outlet channel stretched the droplets in the direction perpendicular to the mean direction of flow (long axis of the device). In addition, fluids between the droplets flowed out from the regions between the droplets to the sides of the HSC, and kept droplets stretched as they flowed downstream. Representative dimensions are 100–200 μm for the width of the inlets ($w_{in}$), 200–500 μm for the width of the orifice ($w_{or}$), 800 μm–2 mm for the length of the orifice ($l_{or}$), 2–5 mm for the width of the outlet channel ($w_{out}$), and 40–80 μm for the height of the device ($h$).

shape of the channel, especially the shape of the HSC. Second, we could control the aspect ratio of the HSC relatively easily during the fabrication of the master. We fabricated the HSC with a wide (2 to 5 mm) and short (height 50 to 100 μm) outlet channel. Third, replica molding made it easy to prepare multiple identical devices; the experiments required testing a range of different fluids. When we tested a different set of surfactants, for example, we had to use a device that was never exposed to the previous set of fluids. Replica molding made it possible to prepare multiple, unused devices that were indistinguishable; the techniques were therefore ideal for the experiments described here.

### Choice of fluids

We used hexadecane as the continuous phase and water as the dispersed phase. The continuous phase must prevent: i) the coalescence of the dispersed phase, and ii) the wetting of the wall of the PDMS channel by the dispersed phase. A solution of Span 80 in hexadecane meets these two criteria (when water is the dispersed phase). Span 80 is an inexpensive, commercially available surfactant; the molecule is an ester of oleic acid that dissolves only in hexadecane, not in water. The use of fluorocarbon or silicone oil, with commercially available surfactants, caused aqueous droplets to coalesce in the HSC when the droplets contacted one another. We chose water as the dispersed phase (*i.e.* droplets). Water is one of the most common liquids used in microfluidics. We studied the effects of additives in the dispersed phase, such as surfactants and other small molecules that changed the physical properties (especially the interfacial free energy) of the droplets, on the behavior of the flowing droplets in the channel. We tested three surfactants (Tween 20, cetyltrimethylammonium bromide, and sodium dodecyl sulfate) that dissolved only in water, not in hexadecane. Our observations indicated that, with the set of fluids and surfactants that we investigated in this manuscript, surfactants must be present in both phases in order to achieve interfacial tensions sufficiently low for droplets to undergo the observed deformations and instabilities during their flow in the HSC in our system.

## Results and discussion

### Notations

Unless otherwise noted, we use the following conventions to describe the system throughout the manuscript. The volumetric rates of flow of the dispersed phase ($Q_d$) and the continuous phase ($Q_c$) are given in square parentheses, denoted as [$Q_d$ (μL s$^{-1}$), $Q_c$ (μL s$^{-1}$)]. The types and concentrations of the surfactants in each phase are given in curved parentheses, denoted as (dispersed fluid, type of surfactant, concentration percentage by weight (w/w); continuous fluid, type of surfactant, concentration percentage by weight (w/w)).

### Formation of the droplets

Many recent studies reported formation of droplets[3,29,30] and bubbles[2,4] in microfluidic flow-focusing devices. Here we only sketch the process that forms the droplets. The flow-focusing region comprises three inlet channels—two side channels for the continuous, organic phase, and a central channel for the dispersed, aqueous phase. The pressure drop across the orifice causes the aqueous thread to advance downstream, to break and emit a droplet, and to retract back. This cycle repeats periodically, and the system generates nearly monodisperse droplets; the coefficient of variation of the diameter of the droplets generated in our current design (defined as the ratio of the standard deviation and the average of diameter) was 5.5% ($n = 30$). A droplet travels downstream in the orifice and reaches the outlet channel. Fig. 2 illustrates the formation and translation of droplets in the flow-focusing geometry, and at the entrance of the HSC.

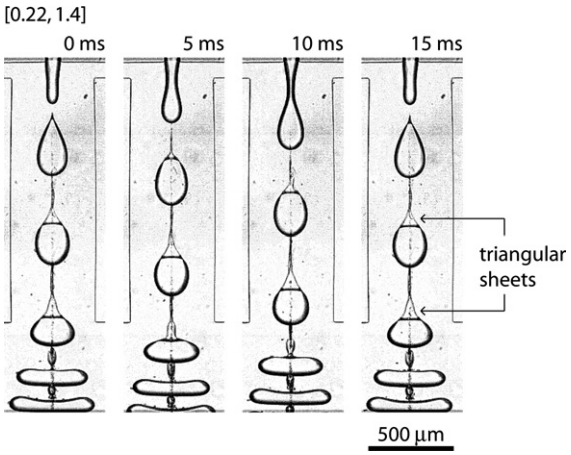


**Fig. 2** Optical micrographs (top view) of the orifice channel illustrating the process by which aqueous droplets formed in the continuous phase of hexadecane, translated in the orifice, and entered the HSC. The set of fluids was (water, Tween 20, 2%; hexadecane, Span 80, 3%). Note that shear forces pulled triangular sheets from translating droplets at the locations where the droplets contacted the top and bottom walls of the channel; Fig. 5a provides a schematic representation of three-dimensional shapes of the droplet.

For the rates of flows we examined, the system produced droplets when the ratio of the rates of flow of the continuous phase (hexadecane; $Q_c$) to the dispersed phase (water; $Q_d$) is $\sim 1 < Q_c/Q_d < \sim 6$. When $Q_c/Q_d$ was much greater than 6, the pressure created by hexadecane pushed water back into the inlet, and the entire device filled with hexadecane. When $Q_c/Q_d$ was less than 1, water flowed through the orifice without break-up; these patterns of flow formed a laminar co-flow of water and hexadecane. Further increase in the rate of the flow of water ($Q_c/Q_d \ll 1$) caused water to flow into the inlets of hexadecane. Fig. 3 shows the phase diagram of the different experimental observations as we varied the two rates of flow (*i.e.* $Q_c$ and $Q_d$); the lines for $Q_c/Q_d = 1$ and $Q_c/Q_d = 6$ are indicated.

### Formation of patterns in an HSC

As the two fluids left the orifice, the streamlines of the continuous phase diverged from the centerline to the sides of the HSC. A single-phase fluid flowing in this configuration would develop streamlines similar to a two-dimensional source flow because the HSC was significantly wider (2 to 5 mm) than the orifice (200 to 500 μm). The streamlines that diverged to the sides of the HSC applied shear stresses on the droplets. As a result, the droplets stretched into elongated shapes characterized by a high aspect ratio (width to length). The continuous phase also flowed out to

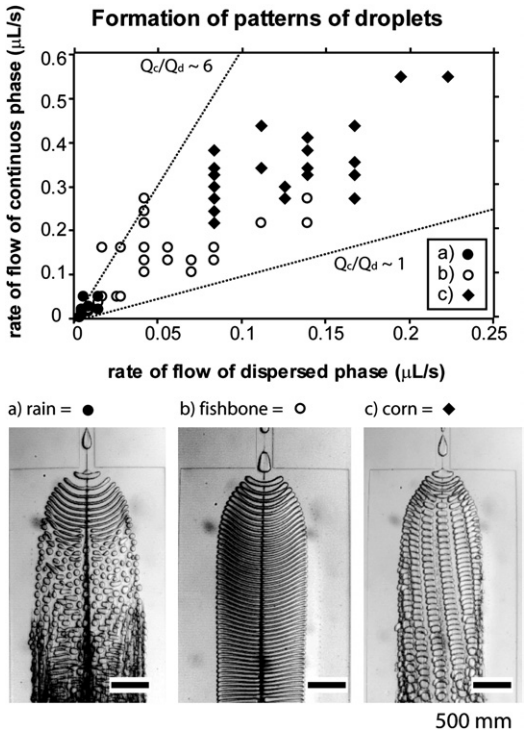


**Fig. 3** A diagram representing the rates of flow of dispersed phase and continuous phase, and the patterns observed for the droplets. The dimensions of the device were $w_{in} = 100$ μm, $w_{or} = 200$ μm, $l_{or} = 800$ μm, $w_{out} = 2$ mm, and $h = 50$ μm, where the parameters are defined in Fig. 1. The set of fluids was (water, Tween 20, 2%; hexadecane, Span 80, 3%). a) *Rain*: stretched droplets broke up into circular droplets *via* capillary instability. b) *Fishbone*: stretched droplets flowing downstream retained the elongated shape. c) *Corn*: stretched droplets periodically broke up into ordered arrays of droplets.

the sides from the regions between the droplets because the droplet traveled more slowly than the surrounding continuous phase; droplets experience higher resistance to flow than the continuous phase.[31,32] The continuous fluid flowing out to the sides of the device from the regions between the droplets further stretched the droplets. Fig. 1b provides a schematic illustration of the streamlines in our HSC. The stretched droplets flowed downstream and formed a regular array.

We divided the patterns formed by the stretched droplets in the HSC into three types (Fig. 3). The pattern that formed depended on the rates of flow of the two fluids. The diagram in Fig. 3 summarizes the rates of flow of the continuous and dispersed phases and the patterns of droplets that formed for a particular device. (We have provided the specifications of the dimensions of the device in the figure caption.) At low rates of flow ($Q_d$ (μL s$^{-1}$) < ~0.01, $Q_c$ (μL s$^{-1}$) < ~0.05) the development of the instability and the break-up of the elongated droplets was faster than the flow of the droplets down the HSC; in this regime, we observed irregular patterns of circular droplets with diameters on the order of the height of the HSC (Fig. 3a; "rain"). At higher rates of flow (~0.01 < $Q_d$ (μL s$^{-1}$) < ~0.08, ~0.05 < $Q_c$ (μL s$^{-1}$) < ~0.25), the elongated droplets traveled all the way through our observation window before they broke up, and we observed regular patterns of arrays of droplets (Fig. 3b; "fishbone"). At even higher rates of flow (~0.08 < $Q_d$ (μL s$^{-1}$) < ~0.2, ~0.25 < $Q_c$ (μL s$^{-1}$) < ~0.6), the droplets formed highly regular patterns in the lateral direction (Fig. 3c; "corn"). In this regime the volume fraction of the droplets in the continuous phase was typically higher than that at lower rates of flow, and the interactions between the droplets led to the formation of the patterns. Since the range of rates of flow characteristic to each regime is different, the typical frequency of generation of droplets is also different in each regime. The typical frequencies of the generation of droplets were 10, 60 and 200 (in droplets generated per second) in the "rain", "fishbone", and "corn" regime, respectively.

### Transition between patterns

We observed transitions among patterns with increasing rates of flow, from the "rain" pattern to the "fishbone" pattern, then to the "corn" pattern. In the following sections, we describe these three patterns and discuss the transitions between these patterns, and mechanisms that led to them in greater detail.

### "Rain"

The "rain" pattern occurs as the result of Rayleigh–Plateau instability, or capillary instability, that occurs with stretched droplets. The stretched droplets were usually slightly wider than the height of the channel, and the width in the direction of flow was on the order of the height of the cell. Confinement of the droplets by the top and bottom walls of the HSC slowed the process of break-up. Confined, or squeezed, immiscible threads exhibit greater stability to the Rayleigh–Plateau instability than do unbounded immiscible threads in a bulk fluid. The wavelength of the most unstable perturbation for the Rayleigh–Plateau instability increases, and the speed of collapse decreases, with increasing confinement.[7,8] Nonetheless, at low rates of flow ($Q_d$ (μL s$^{-1}$) ≈ 0.01, $Q_c$ (μL s$^{-1}$) ≈ 0.05), the stretched droplets slowly developed instabilities, and broke up into smaller droplets as they flowed downstream (Figure S1a; supplemental material†). The resulting patterns were disordered, and the droplets resembled raindrops sliding down a window. The size of the droplets resulting from this break-up process was on the order of the width of the elongated mother droplets; that is, comparable to height of the HSC (50 μm).

### "Fishbone"

At higher rates of flow, droplets remained stretched for a sufficient interval (~3 sec) to travel the entire length of the HSC (2 cm). Two reasons explain the transition from the "rain" regime to the "fishbone" regime: (1) *Volume of individual droplets.* In our Hele-Shaw cell, droplets remained squeezed by the walls in the cell; the larger the volume of droplets, the more significant the effects of the confinement that slowed down the progression of the Rayleigh–Plateau instability, because the cross section of the droplets deviated further from the circular shape. The onset of capillary instability was also suppressed by the neighboring droplets; the wider droplets in the front and back provided additional confinement to the stretched droplet in the middle. For those two reasons, the volume of individual droplets played a role in the suppression of Rayleigh–Plateau instability in the HSC. (2) *Rate of flow.* As the total rate of flow in the "fishbone"

 

regime was ~10 times higher than that in the "rain" regime, the droplets remained in the HSC for a much shorter time. As the result, droplets could exit the channel before the instability became observable. In a straight HSC, the droplets straightened out as they flowed down the channel. We demonstrated that the structure of patterns of droplets could, to some extent, be modulated through changes in the shape of the HSC (Figure S2; supplemental material†).

### "Corn"

As we increased the rates of the flow, we again observed break-up of the elongated droplets. We believe that the transition from the "fishbone" regime to the "corn" regime is due to the increase in the rate of flow and the shear stress. Figure S3 (supplemental material) shows the upper limit of the "fishbone" regime.† The increase in the total rate of flow entering the cell caused the stretched droplets to *bend* more significantly than in the "fishbone" regime. In addition, the shear stresses exerted by the continuous fluid entering the HSC and flowing out to the sides from the regions between the droplets accelerated elongation of the droplets; the elongation 'thinned' the width of the kink on the droplet, then facilitated the onset of capillary instability at the kink. As the break-up of one droplet took place, the cascade of correlated break-up of subsequent droplets followed.

Fig. 4 displays the progression of the events that led to the formation of this pattern. In this regime, the volume fraction of the droplets in the HSC was higher than in the two other regimes that we observed at lower rates of flow (*i.e.* rain and fishbone). The neighboring droplets interacted, and the development of capillary instability was influenced by the confinement introduced by the shape of neighboring droplets. The system of droplets developed a regular pattern of necks and bulges as they elongated and traveled down the channel. The 'necks' in one elongated drop fitted with 'bulges' in the two neighboring (preceding and following) droplets. The resulting restriction for the location of the nodes on the neighboring droplets, and the close interaction between the droplets, created periodic flows (sequence of break-up events), and produced regular arrays of droplets as described in the series of images in Fig. 4.

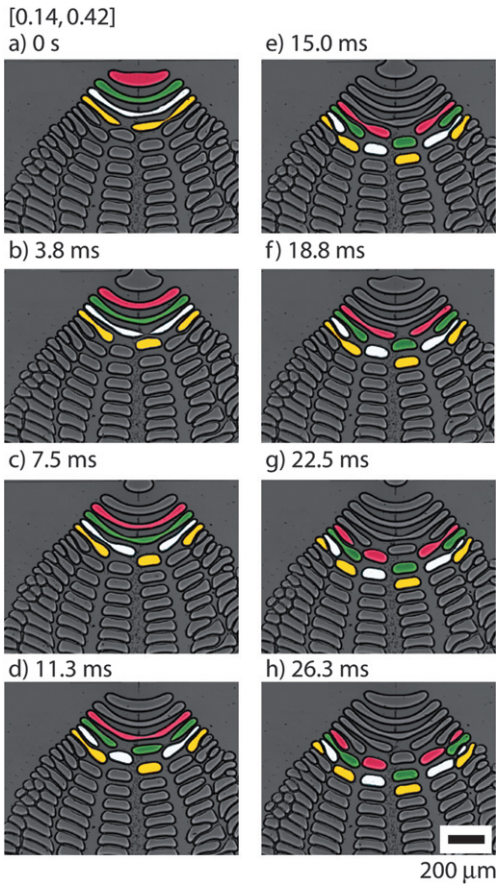


**Fig. 4** Optical microscope images showing the progression of break-up of droplets. The set of fluids was (water, Tween 20, 2%; hexadecane, Span 80, 3%). We colored the droplets in the micrographs using Adobe Photoshop C2; droplets of the same color (red, green, white, and yellow) indicated those which originated from the same mother (original) droplets.

### The shear driven instability

As the drops flowed from the orifice and down the outlet channels, they underwent a second type of instability. The shear stress exerted on the traveling droplets by the floor and ceiling of the HSC dragged liquid 'curtains' of the dispersed phase from the trailing edges of the droplets. These curtains subsequently transformed into arrays of liquid threads—visually akin to a 'comb'—and these threads subsequently broke up into droplets that were much smaller than the height of the HSC. We propose that shear stress causes this instability, and discuss the mechanism of the instability in the following sections; we have called this observation a "shear-driven instability" (SDI).

Shear stress acted in the direction opposite to the direction of the translation of droplets. We postulate that the flow sweeps the surfactant towards the trailing end of the droplets, as it does in the tip-streaming.[26,27] The accumulation of the surfactants at the rear side of the droplets causes the surface tension to decrease at the tail of the droplets, and the shear stress then drags thin liquid threads and sheets from the droplet at the top and bottom walls of the cell. These thin structures subsequently break up into small droplets with diameters at least one order of magnitude smaller than the height of the HSC.

As we increased the rate of flow of the two phases into the HSC, SDI first developed in the orifice channel, where the speed of flow was largest. The black lines in the center of the HSC in Fig. 3b represent very small droplets emitted from the tail of the droplets translating in the orifice. As we further elevated the rates of flow, we also observed SDI in the outlet channel.

### SDI in the orifice channel

As the droplets traveled down the orifice channel, they assumed a tear-drop shape with sharp trailing tails (Fig. 2 and Fig. 5a-i). The tails became wider and developed into two triangular liquid sheets trailing behind the drop, one adjacent to the top and one adjacent to the bottom wall of the cell. When the droplets exited the orifice channel and slowed down, the triangular sheets detached from the droplets (Fig. 5b-i, uppermost droplet). The detached sheets folded into cylindrical threads and later broke up into droplets (Fig. 5b-i and b-ii). We observed the same

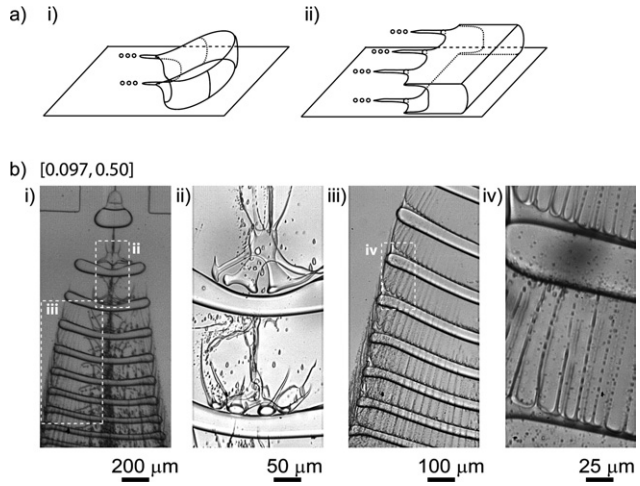


**Fig. 5** a) Schematic illustration of the geometry of the droplets undergoing the shear-driven instabilities in the HSC. i) Shape of the droplet in the orifice channel and ii) portion of the stretched droplet in the outlet channel. For clarity, we sketched only the bottom plate of the HSC, and omitted the top plate. b) Optical micrographs of the HSC illustrating shear-driven instability (SDI) occurring near the ceiling and floor of the HSC ($w_{out}$ = 5 mm). The set of fluids was (water, Tween 20, 2%; hexadecane, Span 80, 3%). i) The triangular liquid sheets pulled behind the droplet in the orifice channel detached at the entrance to the outlet channel. ii) The detached sheets folded into threads and broke into smaller droplets. iii) and iv) As the droplets stretched in the outlet channel, they developed a comb-like structure. The sheets pulled behind the drop developed an array of liquid threads (inset iii), which subsequently separated into smaller drops (inset iv). Note in iv) that the comb structure formed on both the ceiling and the floor of the cell.

instability occurring in the circular droplets formed *via* the capillary instability (*i.e.* "rain" pattern in Fig. 3a).

## SDI in the HSC

The stretched droplets also underwent a similar instability. Two liquid sheets were pulled along the top and bottom boundaries. We observed a periodic shedding of the liquid sheets that subsequently broke into small droplets (Fig. 5b-iii and b-iv). Fig. 5a illustrates this instability schematically. Multiple triangular sheets were pulled from the translating droplets, forming a structure visually similar to a comb, and each triangular sheet went through the same geometrical transformations as those that occurred with tails of circular droplets. We observed that the further were the stretched droplets from the centerline of the channel, the earlier the tails started to emerge (Fig. 5b-iii). These observations reflected the redistribution of the surfactants caused by the flow of the continuous phase *between* the elongated droplets; the flow between the droplets brought the surfactants along the interface toward both ends of the elongated droplets (Fig. 1). As a result, the lateral extremes of the droplets should be expected to have higher concentration of the surfactants at the interfaces than their centers, and the onset of SDI at both ends was enhanced.

The stretched droplets showed higher stability to SDI than circular droplets (Figure S1b; supplemental material†). We believe this stabilization was due to the flow pattern *around* the droplets; when circular droplets traveled, the external flow at both sides of the droplets also facilitated the redistribution of the surfactants to the back of the droplets. The redistribution of the surfactants was thus enhanced more for circular droplets than for stretched droplets. For stretched droplets, a larger number of tails evolved at the ends of the stretched droplets than at the center of the droplet. This observation also suggests that the external flow *around* the stretched droplets enhanced the number of occurrences of SDI. We provide more details about the development of SDI in the supplemental section (Figure S4; supplemental material).†

## Redistribution of surfactants

We suggest possible effects of surfactants in our system, and propose flow patterns that led to the SDI. We believe that the primary cause of the SDI was redistribution of the surfactants around the translating droplets. Accumulation of the surfactants toward the back of the droplet lowered the interfacial tension between water and oil; the decrease in the interfacial tension allowed the shear stresses exerted by the continuous phase recirculating between the droplets to stretch the dispersed phase into thin water films along the top and bottom boundaries of the HSC. These effects are similar to the phenomenon of tip-streaming,[27] and we note that the observed behaviors could not be explained on the basis of capillary numbers calculated with the static values of interfacial tension.

## Flow inside and between droplets and redistribution of surfactant

We propose that the flow pattern inside the traveling drops, and in between two neighboring drops, caused redistribution of surfactant towards the trailing edges of the droplets.[33–36] Such redistribution of surfactants led to the onset of the SDI. Fig. 6 schematically illustrates the flow patterns inside the droplets. In the reference frame traveling with the droplets, the fluid inside the droplet traced convection rolls with positive velocity (in the mean direction of flow) half way between the plates of HSC, and with negative velocity at the walls of HSC. The continuous fluid behind the droplet traced similar patterns with positive speeds in between the plates, and with liquid recirculating back upstream at the top and bottom walls. Note that depending on the viscosities of the two fluids, the actual flow patterns may be more complicated with small regions of closed streamlines near the front and the back of the droplets.

The flow inside the droplets sheared surfactants from the top and bottom interfaces of the droplet towards the trailing ends. The recirculation of the continuous phase from the center of the walls of the HSC sheared surfactant towards the rear top and bottom edges of the droplet. The concentration of surfactant increased, and the interfacial tension decreased at the trailing edge. As a result, the interface yielded to the shear stress exerted by the walls of the HSC, resulting in the onset of SDI. This is the basic scenario commonly described as tip streaming,[27] though here it occurs along a trailing edge. Experiments performed without surfactants in the dispersed phase confirmed the above reasoning: we did not observe the SDI in these experiments (Fig. 6a). We discuss the role of surfactants in the observed instabilities below.

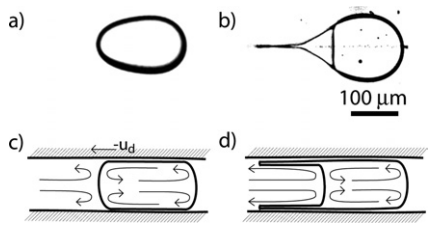


**Fig. 6** a) and b) Optical micrographs (top view) of aqueous droplets in hexadecane containing Span 80 (3%, w/w), traveling in the orifice channel ($w_{or} = 500$ μm). a) A droplet *not* containing any surfactant. In the absence of the surfactant, the droplet preserved an approximately circular cross section. The continuous phase wetted the PDMS wall. b) A droplet containing Tween 20 (2% w/w). In the presence of surfactant, the shear stress exerted by the walls pulled a triangular liquid sheet at the top and bottom walls of the HSC. The surfactants at the interface were sheared to the region of the tail, and the accumulation of the surfactant allowed the formation of the thin film along the wall of the channel. c) and d) Schematic illustrations of the flow in the vertical cross-section of the HSC, for droplets without and with surfactant in the dispersed phase, respectively. The bold lines represent the walls of the HSC and the interface of the droplet, and the arrows show the streamlines of the two fluids in a reference frame traveling with the droplet at a speed $u_d$ (average speed of the velocity of droplets). Flow inside droplets circulates the surfactant toward the trailing end of the droplet, and the flow of the continuous fluid behind the droplet shears surfactant towards the edges at the top and bottom wall. Note that depending on the viscosity ratio between the two fluids the actual flow patterns may be more complicated with small regions of closed streamlines near the front and back of the droplets.

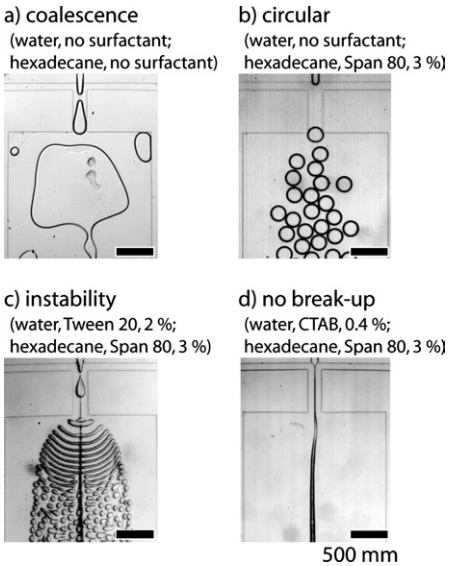


**Fig. 7** Optical micrographs of representative behaviors of aqueous droplets in hexadecane. See the supplemental material for the summary of the behaviors of droplets with varying types and concentrations of surfactants.† a) Coalescence: in the absence of surfactant in the continuous phase, droplets entering the outlet channel coalesced when they made contact. b) Circular: with surfactant present only in the continuous phase, droplets remained in a circular (or discoid) shape in the outlet channel. c) Instability: with surfactant present in both phases, droplets stretched in the outlet channel, and underwent a series of instabilities. The type of instabilities that droplets underwent (*i.e.* rain, fishbone, corn, and SDI) depended on the rates of flow. d) No break-up: droplets did not form in the flow-focusing generator. We observed this regime of the pattern of flow when the concentration of surfactant in the dispersed phase was high.

## Surfactants

We observed the series of instabilities (*i.e.* stretching of the droplets, capillary instability, and SDI) only when surfactants were present in *both* the aqueous and organic phases at sufficiently high concentrations. In order to illustrate the effect of each surfactant, we first varied the presence of surfactants in each phase. The set of fluids and surfactants we used was water with Tween 20 as the dispersed phase, and hexadecane with Span 80 as the continuous phase. These surfactants are only soluble in one phase; Span 80 is soluble in hexadecane, but not in water, and Tween 20 is soluble in water, but not in hydrocarbon.

We first observed that, without Span 80 in hexadecane, aqueous droplets coalesced immediately after they entered the HSC, regardless of the presence of surfactants *inside* aqueous droplets (Fig. 7a): even when the aqueous droplets contained a high concentration of Tween 20 (2% w/w), the droplets still coalesced. As we discuss later, we observed that high concentration of Span 80 (3% w/w) was necessary to allow droplets to stretch. We therefore used a solution of Span 80 (3% w/w) in hexadecane as the "default" continuous phase for the rest of the experiments.

The presence of Tween 20 in aqueous droplets affected the shape of droplets flowing in the outlet channel. At a low concentration of Tween 20 (0.2% by weight or lower), droplets slightly stretched along the diverging field of flow near the entrance of the HSC, but they immediately adopted circular shapes. These circular droplets remained in the circular (or discoid) shape while they flowed in the HSC (Fig. 7b). With sufficiently high concentrations of Tween 20 (2% by weight or greater), we observed that the droplets stretched when they entered the HSC, and went through Rayleigh–Plateau instability (Fig. 7c).

## Spatial variations of the concentrations of surfactants

At low Reynolds numbers, two parallel flow streams that meet undergo laminar flow,[37] and they do not mix by turbulence. This characteristic allows microfluidics to create an environment that has discrete, spatial variations of physical and chemical properties.[38,39] We conducted experiments in which a single phase, either continuous or dispersed, consisted of two different streams, one with a surfactant and the other without a surfactant.

Fig. 8a is a micrograph of the system in which we delivered two streams of the continuous phase into the flow-focusing orifice—one stream with Span 80 (3% w/w), and the other stream without any surfactant. The droplets stretched on the side where Span 80 was present, and they remained circular on the other side. We also observed coalescence of droplets on the side without the surfactant in the continuous phase. In the other two-phase experiment, we formed droplets consisting of two phases of the dispersed fluid—one stream with Tween 20 (2% w/w) and the other with no surfactant (Fig. 8b). In this case, droplets initially stretched to both sides of the HSC, and remained stretched in the side containing Tween 20. In the side without Tween 20, the stretched droplets broke up into smaller droplets and adopted

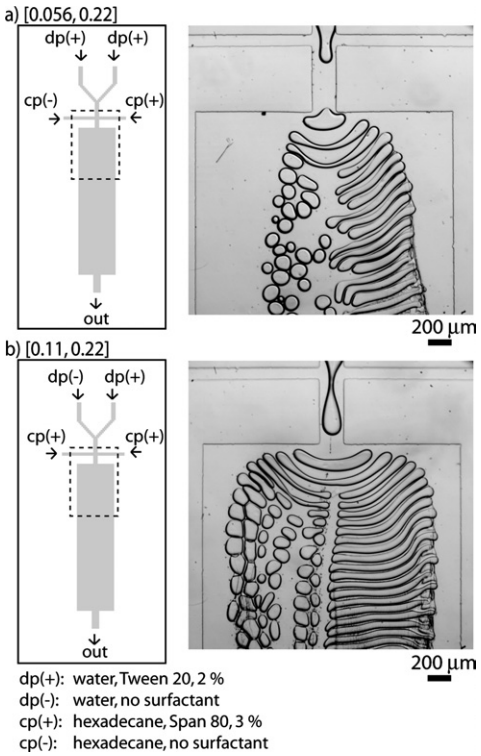


**Fig. 8** Systems in which each phase consists of two streams with different concentrations of surfactant. The type and concentration of the surfactants are specified in the figure. The abbreviations, dp and cp denote dispersed phase and continuous phase, respectively. The signs (+) and (−) denote the presence and absence of respective surfactants for each phase. The indicated rates of flow are the *total* rate of the continuous phase or the dispersed phase. Each phase consists of two streams; the rate of flow of each stream is half of the total rate of flow. a) Only the right half of the continuous phase contains surfactants. b) Only the right half of the dispersed phase contains surfactants.

circular shapes, presumably due to the high interfacial tension. The observations support our original conclusion: in order for droplets to remain stretched, surfactants must be present in both the dispersed phase and continuous phase.

### Effects of surfactants on the interfacial tensions

A low interfacial tension was the key requirement for both the formation of patterns of droplets and the onset of shear-driven instability. As we described in the previous sections, it was necessary to put surfactants in *both* phases to achieve sufficiently low interfacial tensions with the combination of fluids and surfactants that we used. To support our discussion, we measured the interfacial tensions between water and hexadecane with a range of concentrations of Tween 20 and Span 80.

Table 1 summarizes the values of interfacial tension between water and hexadecane measured by pendant drop tensiometry. The use of only one surfactant, either Tween 20 or Span 80, lowered the value of interfacial tension to approximately 5 mN $m^{-1}$, but this value of interfacial tension was not sufficiently low for the instabilities in which we were interested to occur. Simultaneous use of two surfactants allowed us to obtain values of interfacial tension as low as 0.01 mN $m^{-1}$ (a value that we estimated indirectly, as described in the following section); only at this very low value of interfacial tension were we able to observe the series of instabilities that we discussed.

We could not measure the value of interfacial tension by pendant drop tensiometry for the conditions at which we observed the instabilities in which we were most interested (denoted by asterisk in Table 1). Water containing Tween 20 (2–10% by weight) spontaneously dripped into hexadecane containing Span 80 (3% by weight) from the tip of a glass capillary (with a diameter of 1 mm) when the vertical tip was brought into contact with the top surface of hexadecane; we could not obtain stable images of pendant drops at this value of interfacial tension. This observation suggested that the interfacial tension between two solutions was sufficiently low that the interface readily yielded in response to the force of gravity. Such dripping would be observed for high Bond numbers (Bo),[40] reflecting low interfacial tension between two fluids. As we observed similar dripping from a capillary with a smaller diameter (400 μm), we could estimate the interfacial tensions at these conditions to be smaller by a factor of at least 0.16 (=$(400/1000)^2$) than the lowest measured value. Previous studies of the formation of microemulsions also support a large decrease in interfacial tension in water/oil/surfactant ternary systems. The use of co-surfactants is often required to obtain the very low surface tensions that are necessary for the formation of a microemulsion.[41–44]

### Effects of co-surfactants

We varied surfactants and their concentrations inside of aqueous droplets to study the function of co-surfactants. Figure S6 (supplemental material) displays three series of optical micrographs showing break-up and formation of patterns of aqueous droplets with three surfactants: Tween 20, sodium dodecyl sulfate (SDS), and cetyl trimethylammonium bromide (CTAB), respectively.† At low concentrations of surfactants in droplets,

**Table 1** Summary of variation of interfacial tensions between water and hexadecane with varying concentrations of Tween 20 and Span 80, respectively. We were not able to measure the values of interfacial tensions for the sets of concentrations of surfactants denoted with asterisks. The values of interfacial tension are given in mN $m^{-1}$

| | | Concentration of Tween 20 in Water (% w/w) | | | | |
|---|---|---|---|---|---|---|
| | | 0 | 0.02 | 0.2 | 2.0 | 10.0 |
| Concentration of Span 80 in Hexadecane (% w/w) | 0 | 43.16 ± 0.73 | 13.9 ± 0.9 | 7.05 ± 0.03 | 6.87 ± 0.06 | 5.36 ± 0.10 |
| | 0.03 | 6.04 ± 0.22 | 4.44 ± 0.20 | 2.51 ± 0.21 | 2.40 ± 0.38 | 2.54 ± 0.14 |
| | 0.3 | 4.45 ± 0.07 | 1.42 ± 0.18 | 0.67 ± 0.06 | 0.21 ± 0.01 | 0.22 ± 0.00 |
| | 3.0 | 4.05 ± 0.29 | 1.15 ± 0.20 | 0.52 ± 0.03 | * | * |

we obtained spherical droplets. In this regime, the size of the droplets decreased as the concentration of surfactants increased. The lower the interfacial tension became, the more readily the interface yielded to the shear force exerted by the continuous streams. As a result, for a given set of rates of flow, we obtained small droplets with the higher concentration of the surfactant. As we increased the concentration of surfactants further, we observed a series of instabilities. We note that the concentrations of Tween 20 at which we observed the series of instabilities corresponded to those at which the interfacial tensions were too low to be measured by pendant drop tensiometry (Table 1). We believe that the difference in "fishbone" and "rain" patterns in the series of Tween 20 (2% and 10%, respectively) also reflected the size of individual droplets. The effects of confinement that slow down the progress of the capillary instability were less significant for smaller droplets. Here, the use of mixed surfactants with sufficiently high concentrations was again critical for the development of instabilities.

We also studied the effects of non-amphipathic, small molecules: ethanol, glycerol, and trimethylamine n-oxide (TMAO) as co-surfactants in aqueous droplets. None of the systems showed instabilities of the sorts of interest in this paper (Figure S7; supplemental material†).

### Capillary numbers

The lowest volumetric rate of flow at which we observed SDI in the 5 mm wide outlet channel was on the order of $Q \approx 0.01$ μL $s^{-1}$. We estimated the capillary number as $Ca = \mu u/\gamma = \mu Q/wh\gamma \approx 5 \times 10^{-3}$. Here, the parameters were the viscosity of the continuous fluid, $\mu \approx 10^{-3}$ Pa s, the width of the HSC, $w = 5$ mm, the height of the channel, $h = 40$ μm, and the interfacial tension $\gamma \approx 0.01$ mN $m^{-1} = 10^{-5}$ N $m^{-1}$. This value of the capillary number was comparable to the values reported by Kopfsill and Homsy ($Ca \approx 10^{-3}$) and Park *et al.* ($Ca \approx 10^{-2}$) for the formation of sharp trailing ends on bubbles and droplets translating in an HSC.[45,46] The low value of the capillary number suggests that the effects of surface tension dominate the shear stress exerted by the walls of the HSC. We would not expect, however, that sharply pointed threads or liquid sheets could be drawn from the translating drops in flows characterized by these low values of Ca. We therefore believe that capillary numbers based on the static values of interfacial tensions do not explain the observed behaviors of instabilities and changes in the shape of the droplets. We speculate that the accumulation of surfactants at the rear side of the droplets by extensional flows and convection between the droplets lowered the interfacial tension more than it would in the static cases, and allowed the formation of cusps.

## Conclusions

This paper describes the flow of aqueous droplets traveling in a microfluidic Hele-Shaw cell when surfactants significantly influence the behaviors of droplets. This system displayed a range of distinct flow patterns. The combination of flow fields and shear stresses exerted by the continuous fluid caused droplets to elongate perpendicularly to the primary direction of the flow in an HSC; these elongated droplets formed highly regular arrays, and underwent a series of instabilities. The confinement of the droplets by the bottom and top walls of the HSC suppressed the onset of capillary instabilities; as a result, the droplets stayed elongated while they flowed downstream, forming a regular array of droplets. Another type of regular pattern arose at high rates of flow; the interactions between the elongated droplets induced lateral regularities in the events leading to the break-up of elongated droplets, and consequently in the location of the smaller droplets that formed.

### Shear-driven instability

Over a wide range of rates of flow of the two fluids, the droplets developed a shear-driven instability (SDI). This process comprised a cascade of geometrical transformations of the dispersed fluid: from droplets, into thin sheets, to fingers, and finally into small droplets. These small droplets had dimensions that were at least an order of magnitude smaller than the height of the HSC. Based on our observations, we postulate that the SDI resulted from dynamic surface tension effects caused by redistribution of the surfactant along the interface, analogous to tip streaming on isolated droplets in shear and extensional flows. Shear stress played a role at the interface of the liquids due to convective flows both inside the primary droplets (dispersed phase) and in between them (continuous phase). Our microfluidic HSC, combined with a flow-focusing device, offered a convenient experimental setup for studies of multiphase flows and interfacial phenomena such as capillary instabilities and tip streaming.

### Surfactant/co-surfactant system

Droplet-based microfluidic systems involving a single surfactant have been extensively studied, and they are applied in a variety of fields.[47–49] This paper has discussed simultaneous use of two surfactants in droplet-based microfluidic systems. We observed that the interfacial tension between the two fluids was sufficiently low (reduced by a factor greater than 200) to allow extreme elongation of droplets and the formation of trailing films, only when both phases contained surfactants. Extensional flows in these systems could readily modify the shape of the droplets; we demonstrated that a spherical droplet could be stretched to an elongated shape with an aspect ratio (width to length) on the order of 100. While synthesis of non-spherical objects[18,50,51] in microfluidic platforms has been demonstrated, our observation may provide an alternative route to engineer the shape of materials in microfluidics.

### Pattern formations by extensional flows

The most interesting aspect of this work is the observation of a number of instabilities of different origin and the associated mechanisms. The dynamics led to the spontaneous formation of regular patterns. The regularities resulted from: i) extensional flows defined by the geometry of the channel, and ii) extensional flows defined by the other droplets. For example, both the diverging flows at the entrance of the HSC and the flows between two neighboring droplets were necessary to create the "fishbone" pattern. The "corn" pattern was a more striking example of the formation of regular patterns resulting from the interaction among neighboring droplets. The break-up of one stretched droplet changed the extensional field of flow, and triggered the

break-up of the next droplets; these two processes alternated, and led to the formation of a regular, complex pattern of droplets. We could control, or at least affect, the pattern that formed with the variation of a limited number of experimentally accessible parameters (*i.e.* rates of flow). In addition to previous demonstrations of pattern formations in out-of-equilibrium systems,[52–56] our current results once again exhibited the potential of microfluidic systems as a convenient testbed for studying formation of regular patterns in dissipative systems; such patterns are often otherwise difficult to obtain.

## Experimental section

### Fabrication of microfluidic devices

We prepared the microfluidic devices using soft lithography.[57] We sealed the polydimethylsiloxane (PDMS) bas relief molds with the channels patterned in them against flat slabs of PDMS; the two pieces of PDMS were plasma-oxidized for one minute, and the substrates were brought into contact to form an irreversible seal.[28] To ensure that the surfaces of the PDMS channels were hydrophobic after sealing, we incubated the sealed microfluidic devices at 120 °C for at least 24 hours after plasma oxidation and sealing.[28] We delivered the two immiscible phases into the microfluidic chip using polyethylene terephthalate tubing (Becton, Dickinson and Company) from digitally controlled syringe pumps (Harvard Apparatus, model PhD2000).

### Fluids

The dispersed phase was water (Millipore, deionized, $\mu = 0.890$ mPa s at 25 °C) containing Tween 20 (Polysorbate 80, 0.1–10% w/w, Aldrich, a nonionic surfactant). The continuous phase was hexadecane (Sigma-Aldrich, $\mu = 3.032$ mPa s at 25 °C) containing Span 80 (sorbitan oleate, 3% w/w, Aldrich, a nonionic surfactant).[58] Unless stated otherwise, we performed experiments with the 'default' concentrations of surfactants: 2% (w/w) Tween 20 in the aqueous phase and 3% (w/w) Span 80 in the continuous fluid. Other surfactants and additives used in the experiment were cetyltrimethylammonium bromide (~99%, Sigma), sodium dodecyl sulfate (J.T.Baker), and trimethylamine *N*-oxide (98%, Aldrich), ethanol (Pharmaco-AAPER) and glycerol (Gibco BRL); they were dissolved in water (Millipore, deionized) on the benchtop to prepare the samples.

### Imaging

A upright Leica DMRX microscope and a set of still (Nicon Digital Camera DXM 1200) and fast-video (Phantom V7) cameras visualized and recorded the behaviors of the system. We used Adobe Photoshop C2, Adobe Illustrator C2, and Adobe Premiere 7.0 for the analysis of images and the preparation of the figures. The colors of the images (Fig. 4) were added using Adobe Photoshop C2.

### Measurement of interfacial tension

We used a pendant drop tensiometry method to measure the interfacial tension between water and hexadecane.[59] A digital camera (Nicon Digital Camera DXM 1200) took still images of pendant drops from glass capillaries (VWR International). We used Adobe Photoshop C3 to enhance the contrast between the droplet and the background of the digital images. We analyzed the images using home-made software developed by the Stone group (Harvard University, School of Engineering and Applied Sciences).

## Acknowledgements

We thank W. D. Ristenpart and E. A. van Nierop for help with the pendant drop tensiometer and related image analysis software. This work was supported by the US Department of Energy under award DE-FG02-OOER45852. Shared facilities funded by NSF under MRSEC award DMR-0213805 were utilized for some of the work. M.H. acknowledges the provision of travel funds from NSF under NSEC award PHY-0117795. P.G. acknowledges financial support from the Foundation for Polish Science and from the Ministry of Science and Higher Education of Poland for the years 2006–2009.

## References

1 H. S. Hele-Shaw, *Trans. R. Inst. Nav. Archit., London*, 1898, **40**, 218.
2 A. M. Gañán-Calvo and J. M. Gordillo, *Phys. Rev. Lett.*, 2001, 87.
3 S. L. Anna, N. Bontoux and H. A. Stone, *Appl. Phys. Lett.*, 2003, **82**, 364–366.
4 P. Garstecki, I. Gitlin, W. DiLuzio, G. M. Whitesides, E. Kumacheva and H. A. Stone, *Appl. Phys. Lett.*, 2004, **85**, 2649–2651.
5 J. Plateau, *Statique Expérimentale et Théorique des Liquides Soumis aux Seules Forces Moléculaires*, Gauthier-Villars, Paris, 1873.
6 L. Rayleigh, *Proc. R. Soc. London*, 1879, **29**, 71.
7 Y. Son, N. S. Martys, J. G. Hagedorn and K. B. Migler, *Macromolecules*, 2003, **36**, 5825–5833.
8 J. A. Pathak and K. B. Migler, *Langmuir*, 2003, **19**, 8667–8674.
9 K. V. McCloud and J. V. Maher, *Phys. Rep.*, 1995, **260**, 139–185.
10 K. C. Taylor and H. A. Nasr-El-Din, *J. Pet. Sci. Eng.*, 1998, **19**, 265–280.
11 M. J. Blunt, M. D. Jackson, M. Piri and P. H. Valvatne, *Adv. Water Resour.*, 2002, **25**, 1069–1089.
12 J. R. Burns and C. Ramshaw, *Lab Chip*, 2001, **1**, 10–15.
13 E. M. Chan, A. P. Alivisatos and R. A. Mathies, *J. Am. Chem. Soc.*, 2005, **127**, 13854–13861.
14 H. Song and R. F. Ismagilov, *J. Am. Chem. Soc.*, 2003, **125**, 14613–14619.
15 K. Martin, T. Henkel, V. Baier, A. Grodrian, T. Schon, M. Roth, J. M. Kohler and J. Metze, *Lab Chip*, 2003, **3**, 202–207.
16 S. Sugiura, T. Oda, Y. Izumida, Y. Aoyagi, M. Satake, A. Ochiai, N. Ohkohchi and M. Nakajima, *Biomaterials*, 2005, **26**, 3327–3331.
17 S. A. Khan, A. Gunther, M. A. Schmidt and K. F. Jensen, *Langmuir*, 2004, **20**, 8604–8611.
18 S. Q. Xu, Z. H. Nie, M. Seo, P. Lewis, E. Kumacheva, H. A. Stone, P. Garstecki, D. B. Weibel, I. Gitlin and G. M. Whitesides, *Angew. Chem., Int. Ed.*, 2005, **44**, 724–728.
19 B. Zheng, L. S. Roach and R. F. Ismagilov, *J. Am. Chem. Soc.*, 2003, **125**, 11170–11171.
20 S. Hill, *Chem. Eng. Sci.*, 1952, **1**, 247–253.
21 P. G. Saffman and G. Taylor, *Proc. R. Soc. London, Ser. A*, 1958, **245**, 312–329.
22 R. Krechetnikov and G. M. Homsy, *J. Fluid Mech.*, 2004, **509**, 103–124.
23 G. I. Taylor, *Proc. R. Soc. London, Ser. A*, 1934, **146**, 0501–0523.
24 H. A. Stone and L. G. Leal, *J. Colloid Interface Sci.*, 1989, **133**, 340–347.
25 H. A. Stone and L. G. Leal, *J. Fluid Mech.*, 1990, **220**, 161–186.
26 C. D. Eggleton, Y. P. Pawar and K. J. Stebe, *J. Fluid Mech.*, 1999, **385**, 79–99.
27 C. D. Eggleton, T. M. Tsai and K. J. Stebe, *Phys. Rev. Lett.*, 2001, 8704.

 

28 D. C. Duffy, J. C. McDonald, O. J. A. Schueller and G. M. Whitesides, *Anal. Chem.*, 1998, **70**, 4974–4984.
29 T. Nisisako, T. Torii and T. Higuchi, *Lab Chip*, 2002, **2**, 24–26.
30 Q. Y. Xu and M. Nakajima, *Appl. Phys. Lett.*, 2004, **85**, 3726–3728.
31 H. Wong, C. J. Radke and S. Morris, *J. Fluid Mech.*, 1995, **292**, 71–94.
32 H. Wong, C. J. Radke and S. Morris, *J. Fluid Mech.*, 1995, **292**, 95–110.
33 S. S. Sadhal and R. E. Johnson, *J. Fluid Mech.*, 1983, **126**, 237–250.
34 K. J. Stebe, S. Y. Lin and C. Maldarelli, *Phys. Fluids A*, 1991, **3**, 3–20.
35 F. Wassmuth, W. G. Laidlaw and D. A. Coombe, *Phys. Fluids A*, 1993, **5**, 1533–1548.
36 K. J. Stebe and C. Maldarelli, *J. Colloid Interface Sci.*, 1994, **163**, 177–189.
37 D. J. Tritton, *Physical Fluid Dynamics*, Oxford University Press, Oxford, 1988.
38 X. Y. Jiang, Q. B. Xu, S. K. W. Dertinger, A. D. Stroock, T. M. Fu and G. M. Whitesides, *Anal. Chem.*, 2005, **77**, 2338–2347.
39 E. M. Lucchetta, J. H. Lee, L. A. Fu, N. H. Patel and R. F. Ismagilov, *Nature*, 2005, **434**, 1134–1138.
40 Bond number (Bo) is defined as $\mathrm{Bo} = \rho g L^2/\gamma$, where $\rho$ is the density of the fluid, $g$ is the acceleration due to gravity, $L$ is the characteristic length scale of the system, and $\gamma$ is the interfacial tension. Bond number is a measure of importance of the gravitational force relative to the force by the interfacial tension.
41 P. G. de Gennes and C. Taupin, *J. Phys. Chem.*, 1982, **86**, 2294–2304.
42 I. Szleifer, D. Kramer, A. Benshaul, D. Roux and W. M. Gelbart, *Phys. Rev. Lett.*, 1988, **60**, 1966–1969.
43 B. Farago, D. Richter, J. S. Huang, S. A. Safran and S. T. Milner, *Phys. Rev. Lett.*, 1990, **65**, 3348–3351.
44 R. Nagarajan and E. Ruckenstein, *Langmuir*, 2000, **16**, 6400–6415.
45 A. R. Kopfsill and G. M. Homsy, *Phys. Fluids*, 1988, **31**, 18–26.
46 C. W. Park, S. R. K. Maruvada and D. Y. Yoon, *Phys. Fluids*, 1994, **6**, 3267–3275.
47 P. Garstecki, A. M. Gañán-Calvo and G. M. Whitesides, *Bull. Pol. Acad. Sci.*, 2006, **53**, 361–372.
48 H. Song, D. L. Chen and R. F. Ismagilov, *Angew. Chem., Int. Ed.*, 2006, **45**, 7336–7356.
49 A. Gunther and K. F. Jensen, *Lab Chip*, 2006, **6**, 1487–1503.
50 A. B. Subramaniam, M. Abkarian, L. Mahadevan and H. A. Stone, *Nature*, 2005, **438**, 930–930.
51 D. Dendukuri, D. C. Pregibon, J. Collins, T. A. Hatton and P. S. Doyle, *Nat. Mater.*, 2006, **5**, 365–369.
52 T. Thorsen, R. W. Roberts, F. H. Arnold and S. R. Quake, *Phys. Rev. Lett.*, 2001, **86**, 4163–4166.
53 J. P. Raven, P. Marmottant and F. Graner, *Eur. Phys. J. B*, 2006, **51**, 137–143.
54 T. Beatus, T. Tlusty and R. Bar-Ziv, *Nat. Phys.*, 2006, **2**, 743–748.
55 P. Garstecki and G. M. Whitesides, *Phys. Rev. Lett.*, 2006, **97**, 024503.
56 M. Hashimoto, P. Garstecki and G. M. Whitesides, *Small*, 2007, **3**, 1792–1802.
57 Y. N. Xia and G. M. Whitesides, *Annu. Rev. Mater. Sci.*, 1998, **28**, 153–184.
58 D. R. Lide, *Handbook of Chemistry and Physics*, CRC Press, Inc., 77th edn, 1996.
59 Y. Rotenberg, L. Boruvka and A. W. Neumann, *J. Colloid Interface Sci.*, 1983, **93**, 169–183.